Ecosystems
https://doi.org/10.1007/s10021-018-0311-8

Estimating Ecosystem Metabolism to Entire River Networks

Tamara Rodríguez-Castillo,* Edurne Estévez, Alexia María González-Ferreras, and José Barquín

Environmental Hydraulics Institute, Universidad de Cantabria, Avda. Isabel Torres, 15, Parque Científico y Tecnológico de Cantabria, 39011 Santander, Spain

Abstract

River ecosystem metabolism (REM) is a promising cost-effective measure of ecosystem functioning, as it integrates many different ecosystem processes and is affected by both rapid (primary productivity) and slow (organic matter decomposition) energy channels of the riverine food web. We estimated REM in 41 river reaches in Deva-Cares catchment (northern Spain) during the summer period. We used oxygen mass-balance techniques in which primary production and ecosystem respiration were calculated from oxygen concentration daily curves. Then, we used recently developed spatial statistical methods for river networks based on covariance structures to model REM to all river reaches within the river network. From the observed data and the modeled values, we show how REM spatial patterns are constrained by different river reach characteristics along the river network. In general, the autotrophy increases downstream, although there are some reaches associated to groundwater discharges and to different human activities (deforestation or sewage outflows) that disrupt this pattern. GPP was better explained by a combination of ecosystem size, nitrate concentration and amount of benthic chlorophyll *a*, whereas ER was better explained by spatial patterns of GPP plus minimum water temperatures. The presented methodological approach improves REM predictions for river networks compared to currently used methods and provides a good framework to orientate spatial measures for river functioning restoration and for global change mitigation. To reduce uncertainty and model errors, a higher density of sampling points should be used and especially in the smaller tributaries.

Key words: spatial modeling; river ecosystem metabolism; primary production; ecosystem respiration; ecosystem functioning; river network; virtual watershed; SSN model.

Introduction

Ecosystem metabolism represents a cornerstone for ecosystem ecology as it includes the total interrelated fluxes that fix (primary production) and mineralize (respiration) organic carbon (C) of all autotrophic and heterotrophic organisms in an ecosystem (Hall 2016). Therefore, river ecosystem metabolism (REM) that fluctuate along river networks is a promising cost-effective measure of ecosystem functioning, as it integrates many different ecosystem processes and is affected by both

Received 6 July 2018; accepted 25 September 2018
Electronic supplementary material: The online version of this article (https://doi.org/10.1007/s10021-018-0311-8) contains supplementary material, which is available to authorized users.
Author contributions: TR-C designed the study, performed the field surveys, analyzed the data, contributed new methods and wrote the paper. EE participated in the design of the study and field surveys, and helped draft the paper. AMG-F participated in the field surveys and data analysis, and helped draft the paper. JB designed and coordinated the study, performed the field surveys and helped draft the paper.
*Corresponding author; e-mail: rcastillot@unican.es

Published online: 22 October 2018

rapid (primary productivity) and slow (organic matter decomposition) energy channels of the riverine food web.

REM is mainly represented by two metabolic processes, gross primary production (GPP) and ecosystem respiration (ER). GPP is the total C fixed by photosynthetic and chemosynthetic aquatic organisms, and ER is the organic C mineralization by all autotrophic and heterotrophic aquatic organisms. The balance of these two processes, considering ER as a negative flux, is net daily metabolism (NDM). NDM is positive when the ecosystem is accumulating or exporting organic C and negative when it is importing organic C (Lovett and others 2006). Most studies estimating REM have dealt with river reach scales focusing on annual estimates (for example, Uehlinger 2006; Dodds and others 2013) or changes along disturbance gradients (for example, Collier and others 2013; Aristi and others 2014; Rodríguez-Castillo and others 2017). However, no studies have attempted to upscale REM estimates from different and separated river reaches to a whole continuous river network, with the exception of Saunders and others (2018), who only estimated GPP for a river network using a multiple linear regression model. Achieving this will allow improving our knowledge about the spatial complexity of biogeochemical patterns and processes in freshwater ecosystems (McGuire and others 2014).

In addition, producing estimates of REM to entire river networks will be very important from both a theoretical and an applied point of view. Theoretically, REM has long been hypothesized to be heterotrophic (ER > GPP) in headwaters, changing toward autotrophy as we move downstream (mid-order reaches) and reverting the pattern in large rivers (Vannote and others 1980). Current empirical studies based on river reach estimates of REM demonstrate this (McTammany and others 2003; Hall and others 2016), although there are others that have found different patterns (Meyer and Edwards 1990; Young and Huryn 1996). In this regard, characterizing REM spatial patterns at a whole river network scale would be very valuable to better understand the drivers determining spatial patterns of river ecosystem functioning (see Thorp and others 2006; McCluney and others 2014). Moreover, this will also allow estimating the heterotrophic–autotrophic balance of a whole river network integrating REM rates and areas of all the different river reaches. From an applied point of view, these advances will help improving carbon circulation models and understanding the effects of global change on river functioning (Val and others 2016a, b) and it will assist on prioritizing river reaches for ecosystem functioning restoration (Palmer and Febria 2012).

In recent years, there has been a great development and improvement of spatial statistical models (Ver Hoef and others 2006; Ver Hoef and Peterson 2010; Isaak and others 2014; O'Donnell and others 2014). Spatial statistical models resemble traditional linear models, but allow spatial autocorrelation in the random errors (Peterson and Ver Hoef 2010). Local deviations from the mean are modeled using the covariance between neighboring sites, which represents the strength of spatial autocorrelation between two sites given their separation distance (that is, Euclidean distance). These type of models have been frequently applied to terrestrial ecosystems, but in river ecosystems river reaches are hierarchically structured in a network, with nested catchments and river reaches connected by flow (Campbell Grant and others 2007).

Thus, Euclidean distances might be insufficient to characterize the spatial dependency of river reaches, being necessary to include covariance matrices based on hydrologic distances (that is, distance along the river network between two locations). This takes into account the flow-connected and flow-unconnected relationships, depending on whether or not two points in a river network share flow (Peterson and Ver Hoef 2010; Ver Hoef and Peterson 2010). The use of spatial stream network (SSN) models based on both Euclidean (2D scale) and hydrologic (stream network scale) distances can represent the spatial configuration, longitudinal connectivity, discharge, or flow direction characteristics of a river network (Cressie and others 2006; Ver Hoef and others 2006), increasing accuracy and validity of statistical inferences. SSN models have been successfully applied to model different river ecosystem components such as water temperature (for example, Isaak and others 2014; Ashley Steel and others 2016), water chemistry variables (for example, Ver Hoef and Peterson 2010; Scown and others 2017) and fish populations (for example, Isaak and others 2017). However, none has yet tried to model river functioning rates, as ecosystem metabolism, using this type of models.

In this study, we aim to (1) explore GPP and ER spatial patterns and the main factors controlling these ecosystem processes at a river network scale; and to (2) model GPP and ER rates for all reaches of the river network, obtaining the metabolic balance for the whole river network. Our expectations are that GPP and ER will increase downstream following the expected increase in their most likely

control factors: light reaching the streambed and chlorophyll *a* concentration in the benthic zone for GPP; and GPP, river ecosystem biomass and water temperature for ER (Young and others 2008; Bernot and others 2010; Beaulieu and others 2013). We believe that the overall river network metabolic balance will be heterotrophic, as the selected river catchment has a very well developed forest that provide leaf litter inputs and the area occupied by low order streams is much higher than the main principal courses.

Methods

Study Area

The study area includes the Deva-Cares catchment (1200 km^2), located in northern Spain (Figure 1). Deva River flows 64 km before draining into the Cantabrian Sea, Atlantic Ocean. At the mouth, its interannual averaged flow is 29 m^3/s, ranging between 1.5 and 393 m^3/s. Almost half of the catchment area falls within the ''Picos de Europa'' National Park, which acts as a natural boundary between the Deva River and its main tributary, the Cares River (catchment area equal to 495 km^2).

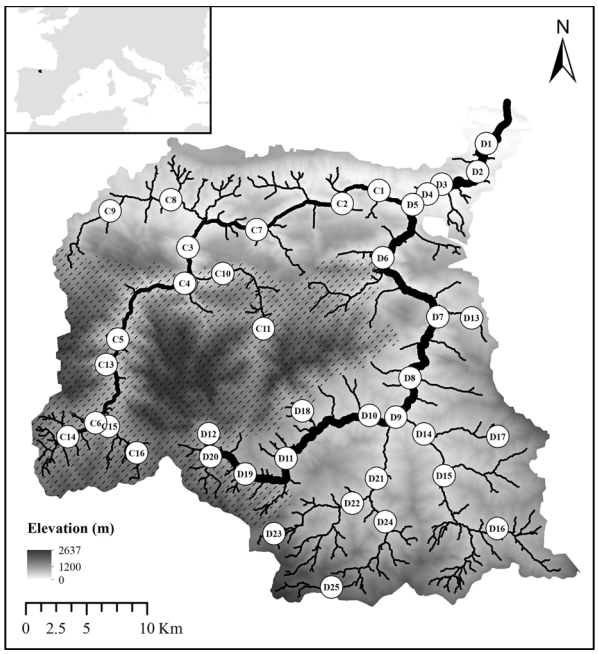

Figure 1. Study area and field reach locations (white points, $n = 41$). The thickest black line represents the Deva River and the second thickest one the Cares River. Dashed lines represent ''Picos de Europa'' National Park. Reach codes are also provided for the Deva (D, $n = 25$) and for the Cares (C, $n = 16$) Rivers.

The ''Picos de Europa'' National Park conditions the catchment geomorphology, with deep and narrow valleys describing sharp curves (that is, boxed meanders). Sandstones and shales predominate in the upper-middle area of the Deva River. In the rest of the catchment, limestone and karst formations dominate. The average altitude is about 1100 m.

The climate is quite variable within the catchment. The temperate oceanic climate predominates (Rivas-Martínez and others 2004), mainly on the coast. Average annual temperature is 14°C, and precipitation is abundant throughout the year with a mean of 1300 mm/year, showing maximum rainfalls in December (150 mm/month) and minimum in July (50 mm/month). There are also important alpine and Mediterranean areas in inner regions, where snow precipitation is frequent above 1000 m.a.s.l. and annual precipitation is much lower (that is, 600 mm/year). In the area, several types of vegetation land cover are present, but beeches and Cantabrian Holm Oaks forests (36%), heaths (31%) and pastures (25%) dominate the landscape.

The population in the catchment amounts to almost 22,000 inhabitants, with a low mean population density (18 inhabitants/km^2) and unequal distribution. Economic activities are based on the agricultural, forestry and services sectors.

Methodological Approach

The main challenges to be addressed when estimating and modeling REM for entire river networks are: (1) the need to break down the river network in relatively homogeneous (size and hydraulic characteristics) river reaches types, (2) the importance of having a wide diversity of predictor variables, and (3) the need to deal with spatial autocorrelation in hydrologically connected river reaches. To accomplish this, we combined a Virtual Watershed approach with a careful spatial field design and the use of SSN models (see below).

Virtual Watershed

A Virtual Watershed (sensu Benda and others 2016) was developed to define the river network and a spatial framework to integrate the predictor variables data necessary for the SSN models (see below). The river network was delineated using flow directions inferred from a 25 m digital elevation model (DEM) with the NetStream software (Benda and others 2007). The river network resulted on 3482 river reaches, with an average length of 500 m (from 16 to 800 m).

Field Design

Catchment area has been shown as one of the most direct and important drivers of flow and river reach hydraulic characteristics for entire river networks (Rodriguez-Iturbe and others 1992; Rodriguez-Iturbe and Rinaldo 1997; Dodov and Foufoula-Georgiou 2004). Therefore, in order to select river reaches to be surveyed throughout the river network, we grouped all river reaches in six catchment sizes (< 10 km^2, 10–40 km^2, 40–150 km^2, 150–400 km^2, 400–1000 km^2, > 1000 km^2). Then we selected a minimum of four and a maximum of nine river reaches within each of the six catchment size categories depending on logistic constrains (budget, accessibility and time in the field), yielding a total of 41 river reaches, 25 along the Deva River and its tributaries, and 16 in the Cares catchment (Figures 1, 2 and steps 1a and 1b in Figure 3). The number of sampling sites was below the recommendation of Isaak and others (2017), but close to the lower limit, allowing to cover and to replicate most of the river hydraulic variability and river ecosystem sizes found in the selected river network. In addition, many other recent studies using SSN models have also used less than 50 sites (for example, Hoef and others 2006; Money and others 2009; Ashley Steel and others 2016; Xu and others 2016; Marsha and others 2018; Neill and others 2018). Field surveys were carried out during the summer of 2014 (August–September, low flow season).

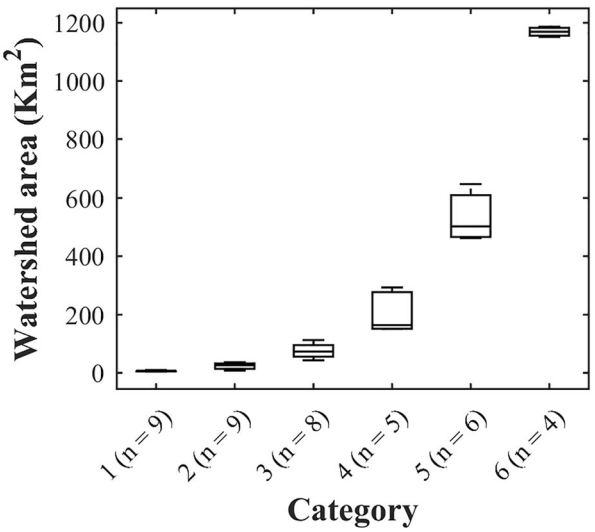

Figure 2. Boxplot for catchment area (km^2) according to the six categories established along the Deva-Cares river network, northern Spain.

Environmental Data

Environmental data were gathered from different sources. First, light reaching the stream benthos, hydraulic characteristics, water quality, and biofilm attributes were surveyed in the selected 41 river reaches concurrently with GPP and ER measures. Second, a set of environmental variables were derived from available GIS layers and linked to the Virtual Watershed, so that all river reaches were attributed with relevant information (see below).

Light and Hydraulic Characteristics

Relative light level (Light) was measured using a HOBO Pendant® Temperature/Light 64 K Data Logger placed on the river bank facing up. The location was chosen to measure average light conditions on the selected river reaches every 5 min for a minimum of 72 h. Percentage of canopy openness (in opposition to riparian cover) was estimated by taking a zenith picture with a fisheye lens and then applying specific software (Gap Light Analyzer, Frazer and others 1999). Because we need predictor variables available for all river reaches in the network, we could not use these estimates. We then used riparian vegetation height and forest cover raster data from LIDAR and satellite images, respectively, derived from previous studies in the area (Álvarez-Martínez and others 2018). We calculated the average vegetation height and forest cover within a 200 m buffer along every single river reach. Both variables correlated with percentage of canopy openness and were used as predictor variables in subsequent analyses.

Total flow (Q), current velocity (V), water depth (D), channel width (W) and cross-sectional area (A) were measured in situ from 5 cross-sectional profiles along the sampling reaches with a Sontek's FlowTracker Handheld ADV. Water velocity and depth were estimated by measuring them on increases of 10% of water width on all transects. Water-surface slope (S) was calculated dividing the length of the reach by the difference in water-surface elevation along the reach.

Water Quality Data

The water physicochemical characteristic was estimated according to Standard Methods for the Examination of Water and Wastewater (APHA and others 1999). Electric conductivity (EC) and pH were measured using an YSI 556 Multi-Parameter Handheld Meter. Water temperature (Tw) and dissolved oxygen concentration (DO), and air temperature (Ta) and barometric pressure (P) were

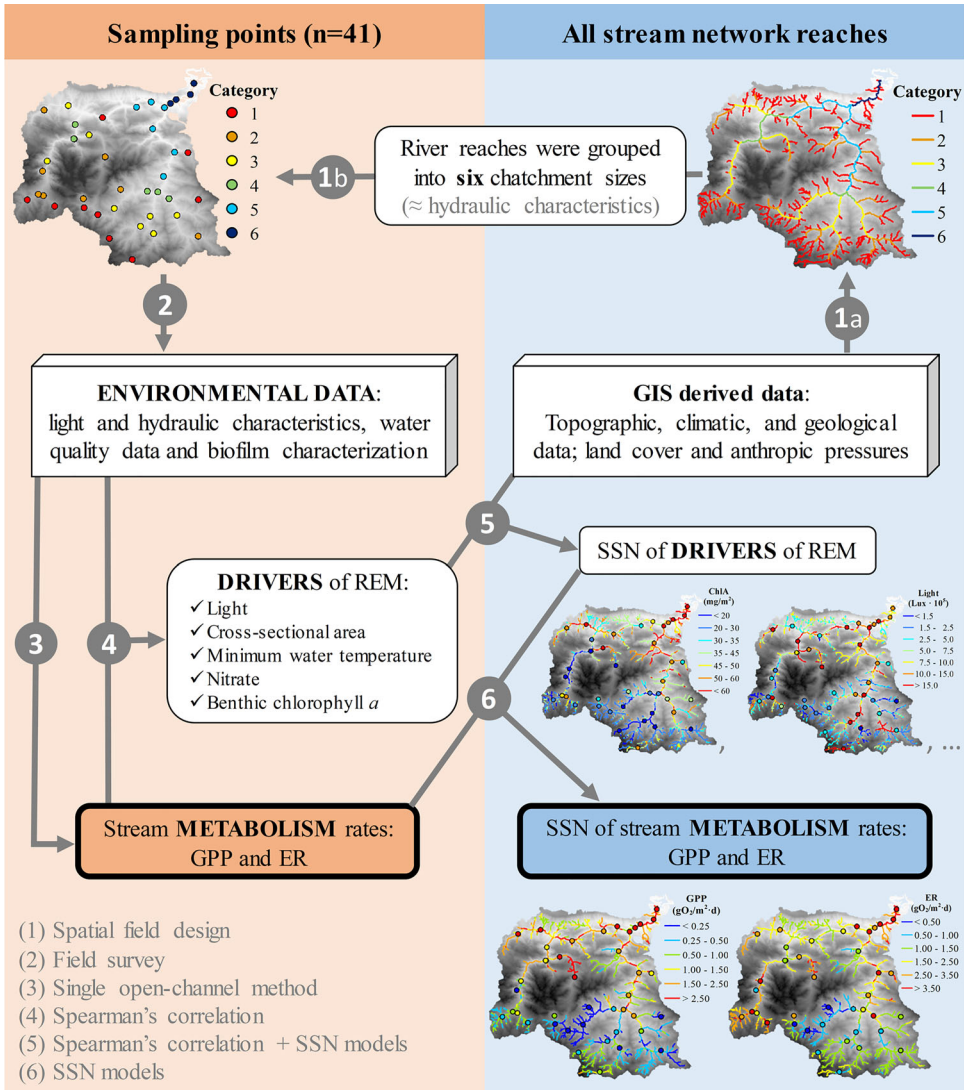

Figure 3. Methodology of work for the development of this study. The tools applied in each step (white numbers) are shown in the lower left corner. In the diagram, two work scales are differentiated, sampling points versus all stream network reaches. *REM* River Ecosystem Metabolism, *GPP* gross primary production, *ER* ecosystem respiration.

monitored every 5 min for a minimum of 72 h using a HOBO Dissolved Oxygen Data Logger and a HOBO 100-Foot Depth Fresh Water Level Data Logger, respectively.

One water sample per reach was collected to determine total suspended solids (TSS), dissolved organic carbon (DOC), orthophosphate (PO4), total organic nitrogen (TON), ammonium (NH4), nitrite (NO2), nitrate (NO3) and silicate (SiO2) concentrations. All water samples were preserved in 250 mL polyethylene containers on ice and transported to the laboratory directly after sampling. TSS were calculated by filtering samples through preweighted standard glass-fiber filters (1 µm) and weighing the residue retained on the filter after dried at 105°C. NO3, NO2, PO4 and SiO2 concentrations were determined by continuous flow analysis and UV spectrophotometry detection (SEAL AA3 HR AutoAnalyzer). NH4 was estimated using continuous flow analysis and molecular fluorescence spectrophotometric detection (SEAL AA3 HR AutoAnalyzer). DOC concentration was determined using catalytic combustion and CO_2 detection with a non-dispersive infrared detector (Shimadzu TOC-V CSH Analyzer). Finally, TON concentration was measured by catalytic combustion and nitrogen monoxide detection by chemiluminescence (Shimadzu TOC-V CSH + TNM-L Analyzer). Values below the detection limit of these

methods were substituted with half of the detection limit.

Biofilm Characterization

To estimate chlorophyll *a* (ChlA) and epilithic biomass (EpB, biofilm organic matter), six cobbles were randomly collected from 3 runs and 3 pools in each sampling reach and frozen at − 20°C until analysis. Then, to extract pigments, these were kept in 90% acetone at 5°C for 24 h in the dark. Absorbance was measured with a Hach-Lange DR-5000 UV-Visible spectrophotometer and pigment concentration (ChlA) calculated following Steinman and others (2007). A revised version of the Sinsabaugh and others (1991) procedure was used to determine the EpB. First, the biofilm was removed from the cobbles by brushing and filtered through a pre-ashed 45-µm glass-fiber filter. Then, this was dried at 95°C, weighed, incinerated at 550°C for 2 h and reweighed to estimate the ash free dry mass. In both cases, stone surface area was estimated by measuring the three longest axes of the stone and applying the equation developed by Graham and others (1988). ChlA and EpB were divided by two as we assumed that only half of the stone total surface area was exposed to light.

Data Derived from Geographical Information Systems

Environmental variables describing several attributes (climate, topography, land cover, geology and anthropogenic alterations) were extracted from existing GIS databases provided by several national and regional organizations. These data have already been analyzed and interpolated to our river network using the NetMap software (Benda and others 2016) in previous studies (see: Peñas and others 2014; Álvarez-Cabria and others 2016; González-Ferreras and others 2016; Table 1).

River Reach Metabolism Estimation

GPP, ER, NDM and production to respiration ratio (*P*/*R* ratio) were calculated following standard methods (Hauer and Lamberti 2007). According to this, NDM is the net change in O_2 concentration per day resulting from biological activity and can be computed as the difference between GPP and ER. The *P*/*R* ratio (GPP/ER) expresses the balance of these metabolic processes in relative terms. If NDM is a positive number and *P*/*R* ratio is greater than 1, there is a net addition of energy to the system (autotrophic state). If the reverse occurs, there is a net loss of energy from the system (heterotrophic state).

In this study, metabolic rates were calculated using the single-station open-channel method. This method is based on the premise that the change in DO (ΔDO) can be attributed to photosynthesis (*P*), respiration (*R*) and gas exchange with the atmosphere (*E*; see equation 1).

$$\Delta \mathrm{DO} = P - R \pm E \tag{1}$$

This change was calculated as the difference between consecutive readings in a point (that is, *i*—(*i* − *t*), being *t* equal to the time step). To estimate the corrected rate of oxygen change (gO_2 m^{-2} day^{-1}), that is, NDM, the differences between dissolved oxygen concentrations were corrected for the DO saturation concentration (C_s), gas exchange with the atmosphere (gas exchange coefficient; K_2) and mean reach depth (see equation 2).

$$\mathrm{NDM}_i = \left(\frac{\mathrm{DO}_i - \mathrm{DO}_{i-t}}{t} - \mathrm{K}_2(C_s - \mathrm{DO}_{i-t})\right) D \tag{2}$$

C_s was obtained from DOTABLES, U.S. Geological Survey software, which calculates C_s from water temperature, barometric pressure and salinity (US-Geological-Survey 2011). The gas exchange coefficient at 20°C and at the measured temperature was determined according to Melching and Flores (1999), following their four equations based on the flow regime (pool and riffle streams and channel-control streams) and flow rate (high and low flow, that is, flow greater or less than 0.556 m^3/s, respectively).

Average night-time respiration (ANR, gO_2 m^{-2} h^{-1}) was calculated as the mean NDM during the night hours. For the photoperiod, this value was corrected for temperature (Thyssen and others 1983), calculating ER (gO_2 m^{-2} day^{-1}) as the sum of respiration for each time step. Therefore, we assumed that instantaneous respiration was constant during the entire day (Bott and others 2006). GPP (gO_2 m^{-2} day^{-1}) was calculated as the sum of diurnal NDM and diurnal respiration (ANR extrapolated to light period). *P*/*R* ratio was calculated as the ratio between GPP and ER.

SSN Models

To model GPP and ER to the whole Deva-Cares river network we followed a modeling approach divided on a series of steps (see Figure 3). First, to select potential drivers of REM, we used the field data (step 2 in Figure 3) to look for those variables that best correlated to the estimated stream metabolism rates (step 3 in Figure 3) using Spearman rank correlation coefficients (step 4 in Figure 3). Then, we estimated these variables to all the non-

Table 1. Environmental Variables Derived from GIS Layers and Attributed to All Reaches of the Deva-Cares River Network

Type	Code	Definition	Units
Topographic	AREA	Drainage catchment area	km^2
	ELEV	Average segment elevation	m
	GRAD	Average segment gradient	m/m
	FLOOD	Flood plain width at 3 × bankfull depths elevations above the channel	m
Climatic	TEMP	Average annual temperature in the segment	°C
	T_ave/max/min_08/09	Average, maximum and minimum monthly temperature (August and September) in the segment	°C
	PREC	Average annual precipitation in the segment	mm
	P_ave/max/min_08/09	Average, maximum and minimum monthly precipitation (August and September) in the segment	mm
	RAD	Average solar radiation in the segment	WH/m^2
Geological	COND	Average conductivity in the segment	1–5*
	PERM	Average permeability in the segment	1–5*
	LIMS	Limestone surface	%
	CLAY	Clay surface	%
	CONG	Conglomerates surface	%
	SDIM	Deposited sediments surface	%
	SHLE	Shale surface	%
	SLIC	Rock silica surface	%
	SLTE	Slates surface	%
Land cover	URB	Urban areas surface	%
	AGR	Agricultural land surface	%
	PAS	Pasture surface	%
	SHR	Shrubs surface	%
	BRD	Broadleaf forest surface	%
	CNF	Coniferous surface	%
	PLN	Forest plantations surface	%
	DND	Denuded areas surface	%
	VEG_H	LIDAR derived riparian vegetation height	m
Anthropic pressures	D_EFFL	Distance to the closest upstream urban or industrial effluent	m
	N_EFFL	Total number of upstream urban and industrial effluents	–

**Quasi-quantitative or ordinal quantitative variables.*

surveyed river reaches (step 5 in Figure 3). To achieve this, we fitted SSN models to each of the main drivers, using as predictor variables the GIS derived data (see Table 1). These predictor variables were also selected using Spearman rank correlation coefficients. Finally, in order to generate predicted values of GPP and ER to all the river reaches in the river network, the results of the SNN models for the main drivers were used to fit the SSN models for the GPP and ER estimates obtained in the field (step 6 in Figure 3). None of the final SSN models used similar or correlated predictor variables among them.

The generation of the SSN models to predict GPP, ER and their main drivers followed a number of consecutive and analogous steps. First, the spatial data needed to fit a stream network model was generated using the Virtual Watershed. This was then edited and formatted in ArcGIS version 10.1 using the spatial tools for the analysis of river systems toolset (STARS; Peterson and Ver Hoef 2014). This preprocessing step created an object (SSN object) which included the geometry and attribute information for the stream network and the observed data in the surveyed reaches.

Secondly, using the R package SSN (version 1.1.10) and following the steps described by Ver Hoef and others (2014), a SSN object was imported into statistical software R (version 3.3.3) to calculate hydrologic distances and to carry out an initial inspection of the obtained torgegrams (semivariances as a function of hydrologic distance for flow-connected and flow-unconnected relationships). It should be noted that the initial inspection of the

GPP and ER torgegrams showed strong and positive spatial autocorrelation at short distances for both flow-connected (increasing variability up to 40 km) and flow-unconnected reaches (increasing variability through all the distance range; Appendix S1: Figures S1a, b).

Thirdly, we restricted our predictor variables to three no-correlated variables (Spearman's correlation coefficient $\leq |0.7|$) as we had 41 observations per response variable. These variables were selected by generating a set of spatial models with all possible combinations of the priori selected potential drivers maintaining a fixed covariance structure and using maximum likelihood (ML) for parameter estimation. Thus, AIC values can be compared, selecting the predictor variables combination with the lowest AIC. Then, a new set of models with predictor variables selected and all possible combinations of the moving average models (tail-up, tail-down and/or Euclidean distance models) and their autocovariance functions was modeled. Covariance parameters were estimated using restricted maximum likelihood (REML). Finally, we choose the spatial model with the lowest AIC value and we checked for outliers, readjusting this when necessary. The final model was used to make predictions with the universal kriging method (Peterson and Ver Hoef 2014).

Finally, a non-spatial (NS) model with the same predictor variables as the final spatial model was also performed for comparison between spatial and non-spatial structure modeled results. Model performance was assessed calculating the root-mean-square percentage error (RMSPE) and the coefficient of determination (R^2) using a leave-one-out cross-validation procedure (that is, removing response values one at a time, and using the estimated model to predict the removed values).

Whole River Network Metabolism Estimation

We multiplied the modeled GPP and ER rates ($gO_2\ m^{-2}\ day^{-1}$ per reach) by the water surface (water width by reach length, m^2) for each river reach ($gO_2\ day^{-1}$ per reach). Daily river network metabolism estimate was the sum of all these reach values ($gO_2\ day^{-1}$ per river network). This global value was divided by the total river network water surface (m^2) to obtain the relative rate, that is, the rate per area ($gO_2\ m^{-2}\ day^{-1}$ per river network).

Data obtained in gO_2 were converted to carbon (or energy) units following Bott (2007). For GPP, we assumed a photosynthetic quotient (PQ, mol O_2 released during photosynthesis/mol CO_2 incorporated) of 1.2 (see equation 3), and for ER we employed a respiratory quotient (RQ, mol CO_2 released/mol O_2 consumed) of 0.85 (see equation 4). Then,

$$gC = gO_2 \times \frac{1}{PQ} \times \frac{12}{32} \quad (3)$$

$$gC = gO_2 \times RQ \times \frac{12}{32} \quad (4)$$

Results

Predictor Variables

In general, Q, D, W and A increased from the smaller tributaries to the larger river reaches, while S showed the opposite pattern and V was higher in the middle-sized river reaches (Table 2). The river reaches in the Cares catchment were characterized by higher V and S than in the Deva catchment, but lower A (Appendix S1: Tables S1 and S2). Light increased from the smaller tributaries to the larger river reaches (although it slightly decreased for category 6), with a greater range of variation for intermediate size categories (Table 2). In addition, higher light values were measured in the Cares catchment than in the Deva catchment, especially for size categories 2 and 4 (Appendix S1: Table S2). Nutrient concentration was also higher in the middle size river reaches (Table 2), showing the reaches in the Cares catchment lower Tw, DOC and SiO2 than those from the Deva catchment, but higher PO4 (Appendix S1: Table S2). ChlA and EpB showed higher values for the two largest size categories (Table 2), without substantially differences between catchments (Table 2).

River Reach Metabolism Estimation

GPP and ER ranged from 0.01 to 6.75 $gO_2\ m^{-2}\ day^{-1}$ (0.003 to 2.11 $gC\ m^{-2}\ day^{-1}$) and from 0.19 to 6.77 $gO_2\ m^{-2}\ day^{-1}$ (0.061 to 2.16 $gC\ m^{-2}\ day^{-1}$), respectively (Appendix S1: Table S1). Both GPP and ER increased exponentially with catchment area (Figure 4A, B; Appendix S1: Table S1), showing a greater dispersion in the Deva catchment than in the Cares catchment (Appendix S1: Table S2). C7 (category 1) and C10 (category 3) showed anomalously high values for GPP (Figure 4A; Appendix S1: Table S1).

NDM and P/R ratio showed a trend toward heterotrophic status in all the surveyed reaches, except in D5, D7, C1, C2, C3, C10, C11 and C12 (Appendix S1: Table S1). NDM and P/R ratio reached lowest values and the greatest dispersion in the

Table 2. Descriptive Statistics (Mean; Standard Deviation, SD; Minimum, Min; and Maximum, Max) for Field Data and Stream Metabolism Rates Estimated for the Six Categories Established Along the Deva-Cares Catchment (see Figure 2), Northern Spain

	Variable		Category 1 (n = 9)				Category 2 (n = 9)			
			Mean	SD	Min	Max	Mean	SD	Min	Max
Light and Hydraulic data	Light	(lux)	748,750	1,316,034	145,827	4,237,114	1,366,525	1,540,522	155,900	4,580,676
	Q	(m^3/s)	0.023	0.018	0.002	0.054	0.087	0.124	0.008	0.401
	V	(m/s)	0.12	0.07	0.03	0.23	0.15	0.08	0.06	0.28
	S	(m/m)	0.050	0.029	0.006	0.094	0.044	0.027	0.013	0.095
	D	(m)	0.14	0.04	0.09	0.22	0.18	0.06	0.09	0.26
	W	(m)	3.26	0.88	1.99	5.04	4.45	2.02	2.55	8.45
	A	(m^2)	0.46	0.20	0.26	0.78	0.91	0.64	0.22	2.20
Water quality data	Tw	(°C)	13.2	1.6	10.3	15.3	12.5	2.6	8.4	15.1
	EC	(µS/cm)	199.1	70.6	77.4	307.0	237.2	38.5	184.9	302.0
	pH		8.46	0.24	8.14	8.85	8.19	0.45	7.70	8.91
	TSS	(mg/L)	25.0	13.7	8.6	46.2	39.4	14.6	19.0	62.0
	DO	(mg/L)	9.36	0.46	8.56	9.89	9.75	0.59	8.68	10.82
	DOC	(µgC/L)	0.87	0.69	0.25	2.48	0.52	0.28	0.25	0.92
	PO4	(µgP/L)	2.5	0.0	2.5	2.5	3.7	3.7	2.5	13.6
	TON	(µgN/L)	161.17	103.01	31.52	343.79	313.59	80.06	171.04	415.14
	NH4	(µgN/L)	10.2	5.0	7.0	20.1	18.9	27.2	7.0	90.0
	NO2	(µgN/L)	0.56	0.28	0.22	1.02	2.17	4.16	0.06	12.90
	NO3	(µgN/L)	160.61	103.08	30.93	343.12	311.42	81.57	170.98	414.34
	SiO2	($\mu gSiO_2$/L)	3274.53	1205.55	1435.81	5082.88	2384.15	1294.32	981.83	4912.62
Biofilm data	ChlA	(mg/m^2)	32.31	16.61	12.49	58.61	36.94	15.21	18.73	56.15
	EpB	(mg/m^2)	5017.1	2676.5	3289.8	12,004.4	8130.9	3318.4	4207.1	12,820.9
	GPP	(gO_2/m^2 d)	0.51	0.55	0.01	1.71	1.25	1.26	0.06	3.53
Stream metabolism rates	ER	(gO_2/m^2 d)	− 1.69	1.37	− 0.19	− 4.04	− 2.08	1.26	− 0.23	− 3.70
	NDM	(gO_2/m^2 d)	− 1.18	1.34	− 3.72	− 0.16	− 0.83	1.35	− 3.08	1.07
	P/R ratio		0.36	0.30	0.07	0.83	0.60	0.56	0.14	1.80

	Variable		Category 3 (n = 8)				Category 4 (n = 5)			
			Mean	SD	Min	Max	Mean	SD	Min	Max
Light and Hydraulic data	Light	(lux)	1,391,202	2,253,497	148,571	6,773,619	1,479,660	1,150,386	233,583	3,287,610
	Q	(m^3/s)	0.229	0.166	0.083	0.490	1.151	1.350	0.053	3.216
	V	(m/s)	0.27	0.12	0.16	0.53	0.32	0.17	0.11	0.59
	S	(m/m)	0.030	0.022	0.008	0.072	0.019	0.009	0.005	0.026
	D	(m)	0.24	0.09	0.12	0.36	0.40	0.26	0.18	0.77
	W	(m)	5.80	1.59	4.18	7.93	9.70	5.12	4.91	18.29
	A	(m^2)	1.43	0.80	0.53	2.61	4.55	4.35	1.23	10.87

Table 2. continued

	Variable		Category 3 (n = 8)				Category 4 (n = 5)			
			Mean	SD	Min	Max	Mean	SD	Min	Max
Water quality data	Tw	(°C)	14.8	1.2	13.2	16.8	14.0	3.2	10.3	18.0
	EC	(µS/cm)	251.5	57.6	188.5	350.0	250.6	80.4	159.6	336.0
	pH		8.49	0.37	7.93	8.93	8.44	0.57	7.68	8.88
	TSS	(mg/L)	43.2	16.3	16.4	67.6	44.2	14.9	32.0	64.8
	DO	(mg/L)	9.55	0.22	9.23	9.77	10.05	0.97	8.85	11.09
	DOC	(µgC/L)	0.65	0.34	0.25	1.40	0.92	1.14	0.25	2.93
	PO4	(µgP/L)	18.8	23.2	2.5	74.0	8.4	5.4	2.5	13.0
	TON	(µgN/L)	464.53	177.39	265.21	749.31	365.05	172.53	162.83	548.95
	NH4	(µgN/L)	27.2	19.7	7.0	73.1	20.3	17.3	7.0	49.2
	NO2	(µgN/L)	2.52	1.83	0.41	6.57	2.48	2.14	0.12	4.91
	NO3	(µgN/L)	462.01	176.71	262.90	747.47	362.57	170.72	162.71	545.01
	SiO2	($\mu gSiO_2/L$)	3838.34	1275.10	2078.87	5563.62	2719.55	1869.98	527.65	4378.61
Biofilm data	ChlA	(mg/m^2)	33.47	28.86	9.50	85.76	27.85	9.90	15.07	42.51
	EpB	(mg/m^2)	5995.7	2988.1	3414.2	10,707.0	6841.2	1542.6	4978.8	8818.1
	GPP	(gO_2/m^2 d)	1.29	1.66	0.16	4.78	1.47	0.66	0.45	2.15
Stream metabolism rates	ER	(gO_2/m^2 d)	− 1.81	1.34	− 0.59	− 4.32	− 1.88	1.11	− 0.87	− 3.68
	NDM	(gO_2/m^2 d)	− 0.52	1.40	− 3.04	2.05	− 0.41	0.77	− 1.72	0.19
	P/R ratio		0.60	0.55	0.17	1.75	0.83	0.29	0.51	1.15

	Variable		Category 5 (n = 6)				Category 6 (n = 4)			
			Mean	SD	Min	Max	Mean	SD	Min	Max
Light and Hydraulic data	Light	(lux)	1,667,326	513,909	1,128,164	2,361,797	1,433,752	524,321	1,017,863	2,186,091
	Q	(m^3/s)	1.842	1.412	0.375	3.825	3.326	0.337	2.924	3.676
	V	(m/s)	0.23	0.06	0.15	0.33	0.20	0.12	0.09	0.37
	S	(m/m)	0.008	0.003	0.003	0.010	0.007	0.005	0.001	0.012
	D	(m)	0.39	0.10	0.28	0.53	0.50	0.31	0.31	0.96
	W	(m)	22.44	12.39	11.71	46.42	33.73	12.53	19.50	47.38
	A	(m^2)	8.38	5.55	2.58	17.99	16.20	8.82	6.84	27.57
Water quality data	Tw	(°C)	17.1	2.6	13.5	20.0	15.9	0.3	15.5	16.3
	EC	(µS/cm)	237.5	41.6	201.0	293.0	257.5	41.5	227.0	316.0
	pH		8.38	0.37	7.98	8.96	8.53	0.34	8.22	8.86
	TSS	(mg/L)	45.8	4.6	39.3	51.6	44.1	5.3	37.6	50.6
	DO	(mg/L)	9.54	0.67	8.81	10.40	9.76	0.10	9.61	9.84
	DOC	(µgC/L)	0.61	0.38	0.25	1.29	4.13	6.64	0.25	14.07
	PO4	(µgP/L)	11.0	5.7	5.6	18.8	6.2	1.0	5.0	7.4
	TON	(µgN/L)	439.73	107.49	327.20	625.63	300.42	16.82	279.92	321.09

Table 2. continued

Variable			Category 5 (n = 6)				Category 6 (n = 4)			
			Mean	SD	Min	Max	Mean	SD	Min	Max
	NH4	(µgN/L)	26.2	4.4	22.5	33.5	27.8	6.2	20.3	35.2
	NO2	(µgN/L)	6.70	6.19	1.96	18.69	2.37	0.47	2.05	3.05
	NO3	(µgN/L)	433.03	101.49	325.24	606.93	298.05	17.22	276.87	319.04
	SiO2	(µgSiO_2/L)	3134.79	1341.01	1557.31	4609.63	1952.07	139.30	1763.85	2060.29
Biofilm data	ChlA	(mg/m^2)	54.50	15.85	31.90	80.31	73.60	13.87	59.01	85.81
	EpB	(mg/m^2)	10,268.6	1920.0	7791.3	13,607.5	12,825.2	324.0	12,575.6	13,261.0
	GPP	(gO_2/m^2 d)	3.06	2.01	1.63	6.75	3.88	0.83	2.77	4.58
Stream metabolism rates	ER	(gO_2/m^2 d)	− 3.40	1.98	− 1.10	− 6.77	− 4.40	1.37	− 2.69	− 6.02
	NDM	(gO_2/m^2 d)	− 0.34	0.98	− 1.79	0.60	− 0.52	0.74	− 1.57	0.07
	P/R ratio		0.97	0.38	0.54	1.55	0.91	0.13	0.74	1.03

Light relative light level, Q total flow, V current velocity, S slope, D depth, W channel width, A cross-sectional area, Tw water temperature, EC electric conductivity, TSS total suspended solids, DO dissolved oxygen, TOC total organic carbon, PO4 orthophosphate, TON total organic nitrogen, NH4 ammonium, NO2 nitrite, NO3 nitrate, Si Silicate, ChlA chlorophyll a, EpB epilithic biomass, GPP gross primary production, ER ecosystem respiration, NDM net daily metabolism, P/R ratio production/respiration ratio.

smallest tributaries (Figure 4C, D; Table 2), whereas the largest river reaches were closer to autotrophy. C10 showed an anomalously high NDM, and C5 anomalously low (Figure 4C; Appendix S1: Table S1).

SSN Models

GPP was influenced ($\rho > 0.45$; Table 3) by A, MinTw, NO3, EpB, ChlA and Light, while ER was related ($\rho > 0.44$; Table 3) to A, MinTw, EpB, ChlA and GPP. Among all these variables, six were selected to enter the modeling approach to predict metabolism for the entire river network: four to predict GPP (A, light, NO3, and ChlA; Table 3) and two to model ER (MinTw and GPP; Table 3). EpB and A were not selected to model ER because they were highly correlated to GPP (Table 3). Thus, the SSN models developed for GPP followed the predictor variables selection described in the methodology; however, only one SSN model was developed for ER as there were only two predictor variables selected.

The SSN models for the selected predictor variables had always a higher coefficient of determination and a lower AIC (except for A and light) and RMSPE than the NS models (Table 4). The coefficient of determination of the SSN models varied between 0.43 for NO3 to 0.71 for MinTw (Table 4; see the rest of cross-validation statistics and model parameters and errors in Appendix S1: Figures S2 and S3, Tables S5 and S6). The covariate model captured a majority of the variability in NS models, except for NO3 (Figure 5A), whereas the spatial covariance functions explained the highest percentage of the variance in SSN models, except for A (Figure 5B). In fact, the residual variation obtained with NS models (Figure 5A) was reduced almost to zero with SSN models (Figure 5B), except for A.

The best model for GPP (lower AIC) was also the SSN model including ChlA, NO3 and A, with ChlA being marginally significant ($p = 0.06$; Table 4). This SSN model reached a 0.69 coefficient of determination and a 0.34 RMSPE (Table 4; see the rest of cross-validation statistics and model parameters and errors in Appendix S1: Figures S2 and S3, Tables S5 and S6). The SSN model for ER presented also a lower AIC value than the NS model, being GPP significant and MinTw non-significant. The coefficient of determination for this SSN model was 0.64, and the RMSPE was 0.95 (Table 4; see the rest of cross-validation statistics and model parameters and errors in Appendix S1: Figure S2 and S3, Tables S5 and S6). The covariate model for GPP and ER captured almost 70% of the

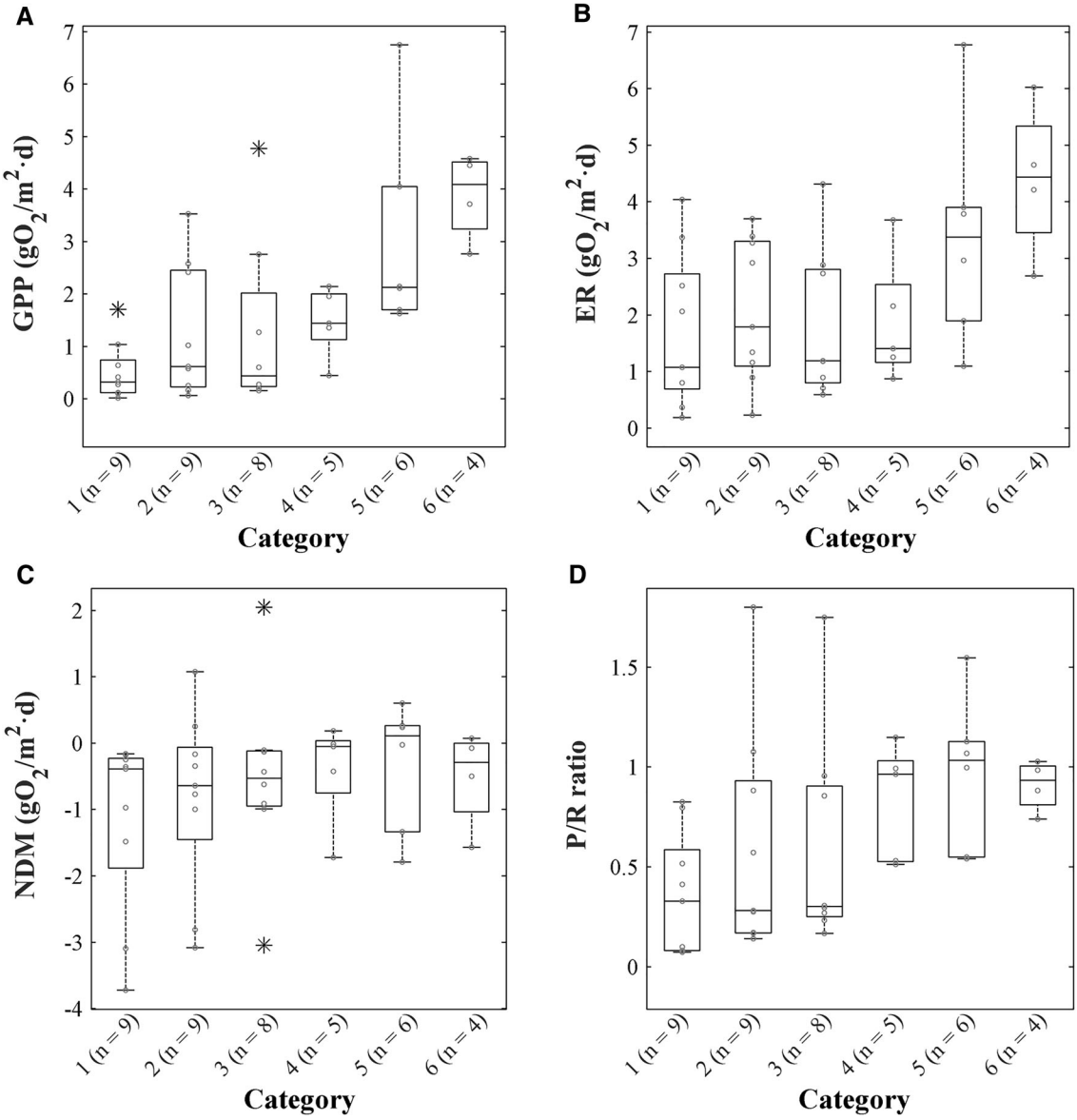

Figure 4. Boxplots for river metabolism rates (GPP = gross primary production, ER = ecosystem respiration, NDM = net daily metabolism, *P*/*R* ratio = production/respiration ratio) according to the six categories established along the river network in the study. Boxplots are for the 25th, 50th (median) and 75th percentiles; whiskers display minimum and maximum values if these are lower than 1.5 times the 25th and 75th percentiles, respectively. Values outside these limits are marked with asterisks. Observed points are marked with gray circles.

observed variability, while the spatial covariance functions explained more than half of the GPP variability but only 30% of the ER variability (Figure 5).

Observed and predicted values obtained with SSN models for predictor variables and metabolism rates showed different patterns along the Deva-Cares river network (Figures 6, 7, respectively). In general, Light, A, MinTw, NO3, ChlA and EpB (Figure 6A–F, respectively) followed a similar pattern with lower values in headwater streams and higher as we move downstream, being this pattern especially clear for A. It is remarkable that light and NO3 showed important increases in some specific reaches of the river network, which could be related to lower riparian cover in the case of light (% of riparian cover in left or right bank $< 33\%$ in D9, D21, D22, D25, C10 and C11; Figures 1, 6A), and sewage effluents in the case of NO3 (upstream sewage effluent distance < 1.6 km in D10, C8 and

Table 3. Summary of the Spearman Rank Correlation Between River Metabolism Rates (GPP and ER) and Potential Drivers

Data type	Variable	ρ_{GPP}	ρ_{ER}
Light	**Light**	**0.57**	–
Hydraulic	***A***	**0.78**	0.55
	D	0.76	0.51
	W	0.74	0.53
Water quality	TSS	0.31	–
	MinTw	0.54	**0.44**
	MeanTw	0.47	0.35
	MaxTw	0.47	–
	pH	0.38	–
	TON	0.48	–
	NO3	**0.48**	–
	NO2	0.34	–
	SiO2	− 0.41	–
Biofilm	EpB	0.70	0.48
	ChlA	**0.68**	0.48
Stream metabolism	**GPP**	–	**0.70**

Bold variables were selected as predictor variables for GPP and ER spatial stream network models. GPP gross primary production; ER ecosystem respiration; Light relative light level; A cross-sectional area; D depth, W channel width, TSS total suspended solids; MinTw minimum water temperature; MeanTw mean water temperature; MaxTw maximum water temperature; TON total organic nitrogen; NO3 nitrate; NO2 nitrite; SiO2 silicate; EpB epilithic biomass; ChlA chlorophyll a Only variables with significant correlation coefficients are shown (p value < 0.05) for the Deva-Cares catchment.

C10; Figure 1, 6D). It is also important to notice the differences in minimum water temperatures from the main Deva (D5 to D8 and D14-D15) and Cares (C1 to C4) river axis, reaching more than to 3°C for a similar catchment area. Finally, ChlA and EpB tended to increase downstream in the Deva catchment, except for some high values (D14, D15 and D25), whereas exceptions in the Cares catchment were much more numerous (C6, C8, C9, C10 and C15).

GPP and ER also showed a general pattern of increasing in downstream direction for the Deva-Cares catchment (Figure 7A, B, respectively), although some headwater reaches showed higher GPP (for example, C10, C11, D25) and ER (for example, C6, C10, C11, C14, C15, C16, D25) values than middle reaches. In general, GPP and ER increased slightly in deforested headwater reaches (similar heterotrophic status that forested reaches, see brown box in Figure 7), except in those reaches affected by effluents (see purple box in Figure 7), where both GPP and ER increased a lot, mainly GPP, reaching an autotrophic status (NDM and *P*/*R* ratio in Figure 7C, D, respectively). On the other hand, in forested headwater reaches with sewage effluents (see green box in Figure 7) only ER increased, increasing the heterotrophic status (NDM and *P*/*R* ratio in Figure 7C, D, respectively).

Whole River Network Metabolism Estimation

GPP for the entire river network was 5.55 t O_2 day^{-1} (that is, 1.73 t C day^{-1}), while ER 7.02 t O_2 day^{-1} (that is, 2.24 t C day^{-1}). NDM was − 1.47 t O_2 day^{-1} (that is, − 0.50 t C day^{-1}), whereas the mean *P*/*R* ratio was 0.79. In relative terms, the Deva-Cares river network produces 1.73 gO_2 m^{-2} day^{-1} (that is, 0.54 gC m^{-2} day^{-1}), but consumes 2.24 gO_2 m^{-2} day^{-1} (that is, 0.70 gC m^{-2} day^{-1}), resulting in a net balance of − 0.46 gO_2 m^{-2} day^{-1} (that is, − 0.16 gC m^{-2} day^{-1}).

Discussion

The combination of field data, Virtual Watershed approach and SSN models has allowed determining REM patterns and the main factors controlling them. This approach has also produced a REM estimation for all the river reaches within the Deva-Cares catchment and for the whole river network. GPP was influenced by river reach cross-sectional area, minimum water temperature, nitrate concentration, biofilm biomass (expressed as ChlA and EpB) and light, whereas ER was related to GPP, river reach cross-sectional area, minimum water temperature and biofilm biomass. The spatial variability of GPP and ER throughout the river network can be accurately predicted from an interplay of these river reach variables using spatial kriging with hydrological distances. We believe that the approach and the results provided in this study certainly help to increase our understanding of how river ecosystem processes are constrained by catchment and river reach characteristics and human impacts.

REM River Network Patterns

In general, the spatial patterns of REM in the Deva-Cares catchment support the theoretical predictions of the river continuum concept (RCC, Vannote and others 1980) that heterotrophy is reduced in the downstream direction, because GPP tends to increase to a greater extent than ER in the middle and lower sections. However, some important deviations from the RCC were noticed. For example, the average NDM and *P*/*R* values were below the autotrophy for all size categories even in the lowest river reaches, which might be characteristic

Table 4. Configuration and Statistic Comparison of SSN and NS Models for All Response Variables

Response variables	Predictor variables	Model type	Moving average models	Autocovariance functions	AIC	RMSPE	R^2
log(Light)	Intercept** SLTE**	NS	–	–	44.51	0.41	0.28
	BRD* CONG**	SSN	Tail-up	Epanechnikow	34.75	0.33	**0.55**
A	Intercept	NS	–	–	228.45	3.82	0.59
	AREA**	SSN	Tail-up	Linear-with-sill	231.15	3.61	**0.62**
Minimum Tw	Intercept** COND**	NS	–	–	167.14	1.78	0.48
	DND** ELEV**	SSN	Tail-up	Linear-with-sill	156.69	1.36	**0.71**
NO3	Intercept**	NS	–	–	505.87	151.69	0.08
	LIMS**	SSN	Tail-up	Linear-with-sill	497.56	120.73	**0.42**
ChlA	Intercept* PREC*	NS	–	–	338.78	16.48	0.44
	PERM** TEMP*	SSN	Tail-up	Epanechnikow	340.36	15.79	**0.49**
EpB	Intercept** PERM**	NS	–	–	725.14	2895.97	0.28
	N_EFFL*	SSN	Tail-up	Linear-with-sill	710.35	2199.40	**0.58**
log(GPP)	Intercept** log(A)**	NS	–	–	49.34	0.41	0.56
	ChlA		Tail-up	Exponential	39.65	0.33	**0.73**
	log(NO3)**	SSN	Tail-down	Linear-with-sill			
log(ER)	Intercept	NS	–	–	10.70	0.24	0.56
	log(GPP)** MinTw		Tail-up Euclidean	Spherical Gaussian	11.37	0.21	**0.67**

The highest R2 value between the NSand SNN models is shown in bold
*Signif. codes: *< 0.05 y **< 0.01.*
A cross-sectional area, MinTw minimum water temperature; NO3 nitrate; ChlA chlorophyll a; EpB epilithic biomass; GPP gross primary production (log-transformed); ER ecosystem respiration. See Table 1 for the explanation of the abbreviation of topographic, climatic, geological, land cover and anthropic pressures data. AIC Akaike information criterion, RMSPE Root-mean-squared prediction error, R^2 coefficient of determination.

of river networks receiving a majority of forest subsidies (for example, Fisher and Likens 1973; Marcarelli and others 2011).

A more detailed analysis of GPP and ER spatial patterns revealed the differential behavior between the Deva and Cares catchments. The first one was clearly heterotrophic along the entire main axis, showing a positive gradient in the downstream direction for GPP and ER. However, the Cares river reaches presented different GPP and ER patterns. GPP was higher in some tributaries that did not correspond to their size category (close to the headwaters), for example, C10, C11, C8 and C9, while ER showed also relatively higher values for these reaches but also for C4, C14, C15 and C16 (Figures 1, 7). We believe that these observed deviations from the general RCC can be explained by the interplay of three key factors: light availability, nutrient availability and water temperature. In this regard, the Deva River maintains a fairly broadleaf forest cover all along its length (limiting light availability), except in the reaches located above the tree line, where the greater light availability favors higher GPP and ER rates (see results within the brown box in Figure 7). Nutrient concentration in the Deva-Cares seems to be related to the geographic structuring of pollution sources (see Appendix S1: Figure S4 for location of sewage outflows in the Deva-Cares and for NH4 and PO4 concentration, and Figure 6 for NO3 concentration), as has been found in other studies (for example, Garreta and others 2009). In addition, the Deva River receives numerous sewage outflows, several of them with a high population equivalent (see Appendix S1: Figure S4), that contribute to increase nutrient concentration (NO3, NH4 and PO4) and biofilm biomass (ChlaA and EpB) as we move downstream (see Appendix S1: Figure S4, and Figure 6D, E, F, respectively). On the other hand, the Cares River receives major contributions

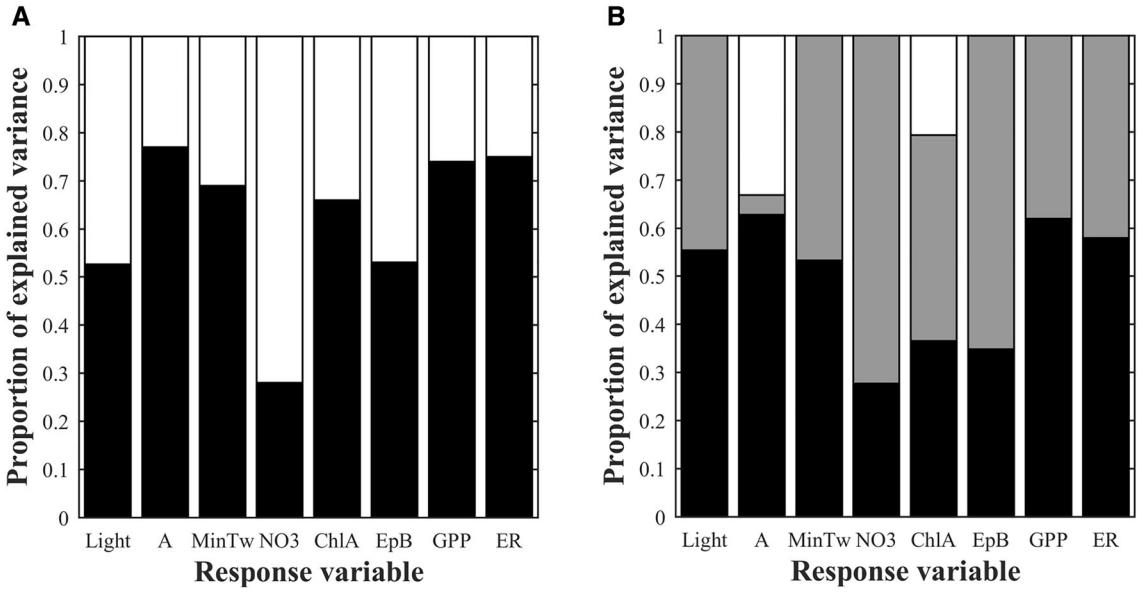

Figure 5. Summary of the proportion of explained variance for the non-spatial (**A**) and spatial models (**B**) selected to predict all the response variables (Light = relative light level; A = cross-sectional area; MinTw = minimum water temperature; NO3 = nitrate; ChlA = chlorophyll *a*; EpB = epilithic biomass; GPP = gross primary production; ER = Ecosystem respiration). Black = covariates; gray = spatial autocovariance functions; white = residuals.

of ground water in the downstream direction (C5 to C2) from many springs that drain the ''Picos de Europa'' central massif (Adrados and others 2010), which might be causing the 3°C difference in minimum water temperature in comparison to river reaches with a similar catchment area in the Deva River (see Appendix S1: Table S4). These lower minimum water temperatures might be lowering ER in the Cares river axis prior to the confluence with the Deva River (Figure 7B). Temperature has also been shown as a major control of ecosystem respiration elsewhere (Beaulieu and others 2013; Smith and Kaushal 2015; Escoffier and others 2016; Saunders and others 2018). Moreover, a conjunction of lower riparian vegetation (higher light flux, Figure 6A) and the presence of sewage outflows (higher nitrate concentration, see Appendix S1: Figure S4, and Figure 6D, respectively) might be responsible for higher GPP and ER in C8, C9, C10 and C11 (see results within the purple box in Figure 7). This positive relationship has also been found in many other studies in the literature (Bernot and others 2010; Finlay 2011; Griffiths and others 2013). However, good riparian cover and the presence of sewage outflows only produced higher ER but similar GPP in C6, C14, C15 and C16 (see results within the green box in Figure 7). Thus, sewage outflows under closed riparian canopies seem to be affecting ER more than GPP rates.

REM River Network Balance

The combination of field observations, Virtual Watershed approach and SSN models has produced an estimate of ecosystem metabolism during the low flow season for the whole Deva-Cares river network. The obtained daily GPP (0.003–2.11 gC m^{-2} day^{-1}) and ER (0.061–2.16 gC m^{-2} day^{-1}) rates for the different river reaches were within the range of values obtained in the literature for other river reach studies (see Hall and others 2016, for a review). However, this study is one of the first attempts to estimate ecosystem metabolism rates integrating all the spatial units of a whole river network, and thus our whole river network estimates can not yet be compared to other approaches.

Other studies have tried to produce global estimates of stream and river metabolism rates by upscaling directly from river reach estimates to the whole surface area that these ecosystems compose globally but without accounting for the spatial variation on river ecosystem rates across river networks (that is, see Battin and others 2008). When we compare our spatialized GPP and ER averages from our whole river network estimates (0.54 and 0.70 gC m^{-2} day^{-1}, for GGP and ER, respectively) to those studies, we observe that our spatialized averages are below the average for both metabolic processes. We believe that this is because

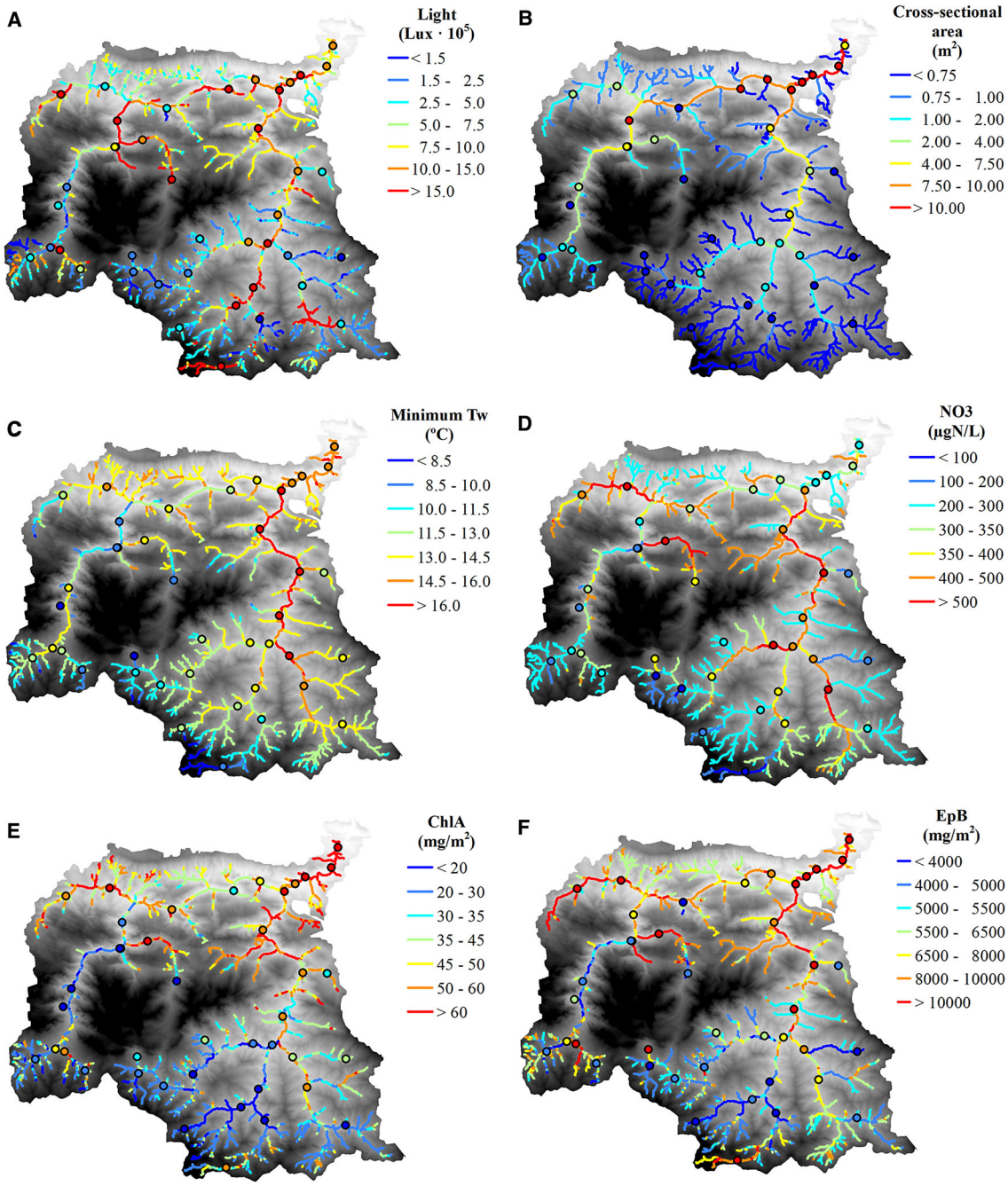

Figure 6. Field data (circles) and predicted values for each reach of the whole river network for relative light levels (Light, map *a*), cross-sectional area (A, map *b*), minimum water temperature (MinTw, map *c*), nitrate (NO3, map *d*), chlorophyll *a* (ChlA, map *e*) and epilithic biomass (EpB, map *f*).

our estimates incorporate the metabolism of all the small tributaries within the Deva-Cares catchment and, thus, produce a much more reliable approach from a spatial point of view. Complementing this spatial approach with REM annual river reach estimates in different river reach size categories will improve the accuracy of REM annual estimates for entire river networks.

Finally, the advantages of the approach we have used in this study is that the contribution of each spatial unit (that is, subcatchments or river reaches) to autotrophy or heterotrophy was spatially explicitly quantified. Thus, this approach could be used to better understand the effects of global change on river networks specifically, but also on global carbon circulation models. This ap-

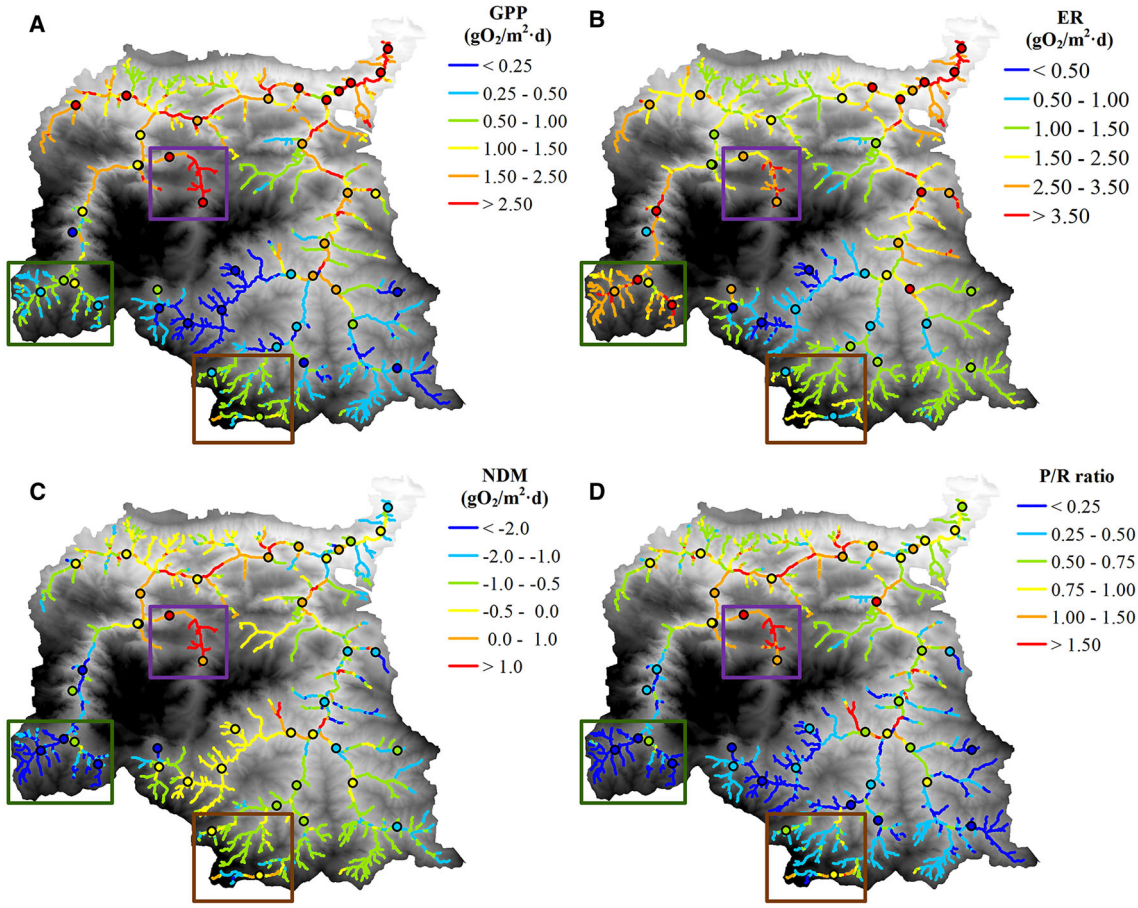

Figure 7. Field data (circles) and predicted values for each reach of the whole river network for river metabolism rates (map *a*, GPP = gross primary production; map *b*, ER = ecosystem respiration; map *c*, NDM = net daily metabolism; map *d*, *P*/*R* ratio = production/respiration ratio). The boxes highlight the headwater reaches subjected to anthropic pressures: deforestation (brown box), effluents (green box), and deforestation and effluents (purple box) (Color figure online).

proach could then be used to model how different management scenarios might change GPP and ER from the reach to the whole river network scales, helping to design future strategies for global change mitigation.

Benefits and Considerations for SSNs Applications

The generation of the statistical theory for stream networks (Peterson and Ver Hoef 2010; Ver Hoef and Peterson 2010) and its integration into friendly usable software (Peterson and Ver Hoef 2014; Ver Hoef and others 2014) has brought important advances to river ecologists. Many different ecosystem attributes can now be modeled for entire river networks (for example, Detenbeck and others 2016; Xu and others 2016; Isaak and others 2017) avoiding the spatial autocorrelation and observation independency and generating information at relevant spatial scales for the study and management of these ecosystems. This is also the case for REM, from which spatial analyses for the Deva-Cares river network allow for recognizing the main environmental problems generating functioning impairment and the possible solutions to fix ecosystem functioning rates.

Our SSN models showed relatively high predictive capacity and produced reliable and logical spatial results, significantly higher than those obtained with non-spatial models. Consequently, this methodology allows us to detect not only the main drivers of REM, but also their spatial patterns. Therefore, we can identify where and how these drivers modify the river ecosystem functioning, what constitutes key knowledge to improve the management of freshwater ecosystems and to be able to develop more complex mechanistic models. However, there are considerations that need to be taken into account when using these models, especially related to the spatial design of the field

observations. In general, it is difficult to determine the optimal distance between observation points to minimize the model errors. For example, in this study, the small tributaries located in the northern fringe of the Cares River and in the southern fringe of the Deva-Cares catchment would need additional information to improve the obtained REM predictions (see error maps in Appendix S1: Figure S3). All those small river reaches currently have no field observations, being the closer (hydrological distance) on a relatively much larger river axis and, thus, GPP and ER estimates would be much more uncertain (Ver Hoef and Peterson 2010; Isaak and others 2017). In fact, SSN developers have recently released a methodology to maximize the spatial design of river networks. This should be carefully considered in future studies and when using data from monitoring networks as it has been suggested by different researchers (Barquín and others 2015; Isaak and others 2017).

Conclusions

In this study, we have determined GPP and ER spatial patterns and the main factors controlling these ecosystem processes for the Deva-Cares catchment and we have also obtained an estimation of ecosystem metabolism for the whole river network. The Deva-Cares river network autotrophy increases downstream, although there are some parts of the river network associated with groundwater discharges (Cares River main axis) and to different human activities (riparian forest clearance or sewage outflows) that disrupt this longitudinal pattern. In general, GPP was better explained by a combination of ecosystem size (river reach cross-sectional area), nitrate concentration and amount of benthic Chl a, whereas ER was better explained by spatial patterns of GPP plus minimum water temperatures. The presented methodological approach improves REM predictions for entire river networks compared to current approaches and provides a good framework to orientate spatial measures for river function restoration and for global change mitigation. To reduce uncertainty and model errors, a higher density of sampling points should be used, especially in the smaller tributaries.

Acknowledgements

This study was partly funded by the Spanish Ministry of Economy and Competitiveness (MINECO) as part of the project HYDRA (REF: BIA2015-71197). José Barquín was supported by a Ramón y Cajal grant (Ref: RYC-2011-08313) of the Ministry of Economy and Science of the Total Environment Competitiveness. We are also grateful to the University of Cantabria for the funding to Tamara Rodríguez-Castillo through a Postgraduate Grant.

References

Adrados L, Alonso V, Bahamonde JR, Farias P, Fernández González LP, Gutiérrez Claverol M, Heredia Carballo N, Jiménez Sánchez M, Meléndez Asensio M, Merino Tomé O, Villa Otero E. 2010. Parque Nacional de los Picos de Europa : guía geológica. 2nd ed. (Adrados Ed., editor.). Instituto Geológico y Minero de España http://j-g-sansegundo.over-blog.es/article-parque-natural-de-los-picos-de-europa-guia-de-geologica-62118095.html.

Álvarez-Cabria M, Barquín J, Peñas FJ. 2016. Modelling the spatial and seasonal variability of water quality for entire river networks: relationships with natural and anthropogenic factors. Sci Total Environ 545:152–62.

Álvarez-Martínez JM, Jiménez-Alfaro B, Barquín J, Ondiviela B, Recio M, Silió-Calzada A, Juanes JA. 2018. Modelling the area of occupancy of habitat types with remote sensing. Isaac N, editor. Methods Ecol Evol 9:580–93. https://doi.org/10.1111/2041-210X.12925.

APHA, AWWA, WEF. 1999. Standard Methods for the Examination of Water and Wastewater 20th edition.

Aristi I, Arroita M, Larrañaga A, Ponsatí L, Sabater S, von Schiller D, Elosegi A, Acuña V. 2014. Flow regulation by dams affects ecosystem metabolism in Mediterranean rivers. Freshw Biol 59:1816–29. https://doi.org/10.1111/fwb.12385.

Ashley Steel E, Sowder C, Peterson EE. 2016. Spatial and temporal variation of water temperature regimes on the snoqualmie river network. JAWRA J Am Water Resour Assoc 52:769–87. https://doi.org/10.1111/1752-1688.12423.

Barquín J, Benda LE, Villa F, Brown LE, Bonada N, Vieites DR, Battin TJ, Olden JD, Hughes SJ, Gray C, Woodward G. 2015. Coupling virtual watersheds with ecosystem services assessment: a 21st century platform to support river research and management. Wiley Interdiscip Rev Water 2:609–21. https://doi.org/10.1002/wat2.1106.

Battin TJ, Kaplan LA, Findlay S, Hopkinson CS, Marti E, Packman AI, Newbold JD, Sabater F. 2008. Biophysical controls on organic carbon fluxes in fluvial networks. Nat Geosci 1:95–100. https://doi.org/10.1038/ngeo101.

Beaulieu JJ, Arango CP, Balz DA, Shuster WD. WD. 2013. Continuous monitoring reveals multiple controls on ecosystem metabolism in a suburban stream. Freshw Biol 58:918–37. https://doi.org/10.1111/fwb.12097.

Benda L, Miller D, Andras K, Bigelow P, Reeves G, Michael D. 2007. NetMap: a new tool in support of watershed science and resource management. For Sci 53:206–19. https://www.researchgate.net/publication/233694439_NetMap_A_New_Tool_in_Support_of_Watershed_Science_and_Resource_Management.

Benda L, Miller D, Barquin J, McCleary R, Cai T, Ji Y. 2016. Building virtual watersheds: a global opportunity to strengthen resource management and conservation. Environ Manag 57:722–39. http://www.ncbi.nlm.nih.gov/pubmed/26645078.

Bernot MJ, Sobota DJ, Hall RO, Mulholland PJ, Dodds WK, Webster JR, Tank JL, Ashkenas LR, Cooper LW, Dahm CN,

Gregory SV, Grimm NB, Hamilton SK, Johnson SL, McDowell WH, Meyer JL, Peterson B, Poole GC, Maurice Valett HM, Arango C, Beaulieu JJ, Burgin AJ, Crenshaw C, Helton AM, Johnson L, Merriam J, Niederlehner BR, O'Brien JM, Potter JD, Sheibley RW, Thomas SM, Wilson K. 2010. Inter-regional comparison of land-use effects on stream metabolism. Freshw Biol 55:1874–90.

Bott TL. 2007. Primary productivity and community respiration. In: Methods in stream ecology. pp 663–90.

Bott TL, Montgomery DS, Newbold JD, Arscott DB, Dow CL, Aufdenkampe AK, Jackson JK, Kaplan LA. 2006. Ecosystem metabolism in streams of the Catskill Mountains (Delaware and Hudson River watersheds) and Lower Hudson Valley. J North Am Benthol Soc 25:1018–44. https://doi.org/10.1899/0887-3593%282006%29025%5B1018%3AEMISOT%5D2.0.CO%3B2.

Campbell Grant EH, Lowe WH, Fagan WF. 2007. Living in the branches: population dynamics and ecological processes in dendritic networks. Ecol Lett 10:165–75. http://www.ncbi.nlm.nih.gov/pubmed/17257104.

Collier KJ, Clapcott JE, Duggan IC, Hamilton DP, Hamer M, Young RG. 2013. Spatial variation of structural and functional indicators in a large New Zealand river. River Res Appl 29:1277–90.

Cressie N, Frey J, Harch B, Smith M. 2006. Spatial prediction on a river network. J Agric Biol Environ Stat 11:127–50. https://doi.org/10.1198/108571106X110649.

Detenbeck NE, Morrison AC, Abele RW, Kopp DA. 2016. Spatial statistical network models for stream and river temperature in New England, USA. Water Resour Res 52:6018–40. https://doi.org/10.1002/2015WR018349.

Dodds WK, Veach AM, Ruffing CM, Larson DM, Fischer JL, Costigan KH. 2013. Abiotic controls and temporal variability of river metabolism: multiyear analyses of Mississippi and Chattahoochee River data. Freshw Sci 32:1073–87. https://doi.org/10.1899/13-018.1.

Dodov B, Foufoula-Georgiou E. 2004. Generalized hydraulic geometry: insights based on fluvial instability analysis and a physical model. Water Resour Res 40:1–15.

Escoffier N, Bensoussan N, Vilmin L, Flipo N, Rocher V, David A, Métivier F, Groleau A. 2016. Estimating ecosystem metabolism from continuous multi-sensor measurements in the Seine River. Environ Sci Pollut Res . https://doi.org/10.1007/s11356-016-7096-0.

Finlay JC. 2011. Stream size and human influences on ecosystem production in river networks. Ecosphere 2:1–21. https://doi.org/10.1890/ES11-00071.1.

Fisher SG, Likens GE. 1973. Energy flow in Bear Brook, New Hampshire: an integrative approach to stream ecosystem metabolism. Ecol Monogr 43:421–39. https://doi.org/10.2307/1942301.

Frazer G, Canham C, Lertzman K. 1999. Gap Light Analyzer (GLA), Version 2.0: Imaging software to extract canopy structure and gap light transmission indices from true-colour fisheye photographs, users manual and program documentation. Program.

Garreta V, Monestiez P, Ver Hoef JM. 2009. Spatial modelling and prediction on river networks: up model, down model or hybrid? Environmetrics 21:439–56. https://doi.org/10.1002/env.995.

González-Ferreras AM, Barquín J, Peñas FJ. 2016. Integration of habitat models to predict fish distributions in several watersheds of Northern Spain. J Appl Ichthyol 32:204–16. https://doi.org/10.1111/jai.13024.

Graham AA, McCaughan DJ, McKee FS. 1988. Measurement of surface area of stones. Hydrobiologia 157:85–7.

Griffiths NA, Tank JL, Royer TV, Roley SS, Rosi-marshall EJ, Whiles MR, Beaulieu JJ, Johnson LT. 2013. Agricultural land use alters the seasonality and magnitude of stream metabolism. Limnol Oceanogr 58:1513–29.

Hall RO. 2016. Metabolism of streams and rivers: estimation, controls and application. In: Stream ecosystems in a changing environment. pp 151–80.

Hall RO, Tank JL, Baker MA, Rosi-Marshall EJ, Hotchkiss ER. 2016. Metabolism, gas exchange, and carbon spiraling in rivers. Ecosystems 19:73–86. https://doi.org/10.1007/s10021-015-9918-1.

Hauer FR, Lamberti GA. 2007. Methods in stream ecology. 2nd edn. Cambridge: Academic Press.

Isaak DJ, Ver Hoef JM, Peterson EE, Horan DL, Nagel DE. 2017. Scalable population estimates using spatial-stream-network (SSN) models, fish density surveys, and national geospatial database frameworks for streams. Can J Fish Aquat Sci 74:147–56. https://doi.org/10.1139/cjfas-2016-0247.

Isaak DJ, Peterson EE, Ver Hoef JM, Wenger SJ, Falke JA, Torgersen CE, Sowder C, Steel EA, Fortin M-J, Jordan CE, Ruesch AS, Som N, Monestiez P. 2014. Applications of spatial statistical network models to stream data. Wiley Interdiscip Rev Water 1:277–94. https://doi.org/10.1002/wat2.1023.

Lovett GM, Cole JJ, Pace ML. 2006. Is net ecosystem production equal to ecosystem carbon accumulation? Ecosystems 9:152–5. https://doi.org/10.1007/s10021-005-0036-3.

Marcarelli AM, Baxter CV, Mineau MM, Hall RO. 2011. Quantity and quality: unifying food web and ecosystem perspectives on the role of resource subsidies in freshwaters. Ecology 92:1215–25.

Marsha A, Steel EA, Fullerton AH, Sowder C. 2018. Monitoring riverine thermal regimes on stream networks: insights into spatial sampling designs from the Snoqualmie River, WA. Ecol Indic 84:11–26. https://www.sciencedirect.com/science/article/pii/S1470160X17305186.

McCluney KE, Poff NL, Palmer MA, Thorp JH, Poole GC, Williams BS, Williams MR, Baron JS. 2014. Riverine macrosystems ecology: sensitivity, resistance, and resilience of whole river basins with human alterations. Front Ecol Environ 12:48–58. https://doi.org/10.1890/120367.

McGuire KJ, Torgersen CE, Likens GE, Buso DC, Lowe WH, Bailey SW. 2014. Network analysis reveals multiscale controls on streamwater chemistry. Proc Natl Acad Sci 111:7030–5. https://doi.org/10.1073/pnas.1404820111.

McTammany ME, Webster JR, Benfield EF, Neatrour M a. 2003. Longitudinal patterns of metabolism in a southern Appalachian river. J North Am Benthol Soc 22:359–70. http://apps.webofknowledge.com.proxy.lib.duke.edu/full_record.do?product=UA&search_mode=Refine&qid=15&SID=3AleLKIb3jNhB@iKGHF&page=4&doc=36.

Melching CS, Flores HE. 1999. Reaeration equations derived from U.S. Geological Survey Database. J Environ Eng 125:407–14. http://www.scopus.com/inward/record.url?eid=2-s2.0-0033133913&partnerID=tZOtx3y1.

Meyer JL, Edwards RT. 1990. Ecosystem metabolism and turnover of organic carbon along a blackwater river continuum. Ecology 71:668–77.

Money E, Carter GP, Serre ML. 2009. Using river distances in the space/time estimation of dissolved oxygen along two impaired river networks in New Jersey. Water Res 43:1948–58. http://www.ncbi.nlm.nih.gov/pubmed/19285333.

Neill AJ, Tetzlaff D, Strachan NJC, Hough RL, Avery LM, Watson H, Soulsby C. 2018. Using spatial-stream-network models and long-term data to understand and predict dynamics of faecal contamination in a mixed land-use catchment. Sci Total Environ 612:840–52. http://www.ncbi.nlm.nih.gov/pubmed/28881307.

O'Donnell D, Rushworth A, Bowman AW, Marian Scott E, Hallard M. 2014. Flexible regression models over river networks. J R Stat Soc Ser C Appl Stat 63:47–63.

Palmer MA, Febria CM. 2012. The Heartbeat of Ecosystems. Science 80:336. http://science.sciencemag.org/content/336/6087/1393.full.

Peñas FJ, Barquín J, Snelder TH, Booker DJ, Álvarez C. 2014. The influence of methodological procedures on hydrological classification performance. Hydrol Earth Syst Sci 18:3393–409. http://www.hydrol-earth-syst-sci.net/18/3393/2014/.

Peterson EE, Ver Hoef JM. 2010. A mixed-model moving-average approach to geostatistical modeling in stream networks. Ecology 91:644–51. https://doi.org/10.1890/08-1668.1.

Peterson EE, Ver Hoef JM. 2014. STARS : An ArcGIS toolset used to calculate the spatial information needed to fit spatial statistical models to stream network data. J Stat Softw 56:1–17. http://www.jstatsoft.org/v56/i02/.

Rivas-Martínez S, Penas A, Díaz TE. 2004. Bioclimatic & Biogeographic Maps of Europe. http://www.globalbioclimatics.org/form/maps.htm.

Rodríguez-Castillo T, Barquín J, Álvarez-Cabria M, Peñas FJ, Álvarez C. 2017. Effects of sewage effluents and seasonal changes on the metabolism of three Atlantic rivers. Sci Total Environ 599–600:1108–18. http://linkinghub.elsevier.com/retrieve/pii/S0048969717311671.

Rodriguez-Iturbe I, Rinaldo A. 1997. Fractal river basins: chance and self-organization.

Rodriguez-Iturbe I, Rinaldo A, Rigon R, Bras RL, Ijjasz-Vasquez E, Marani A. 1992. Fractal structures as least energy patterns: the case of river networks. Geophys Res Lett 19:889–92. http://onlinelibrary.wiley.com/doi/10.1029/92GL00938/abstract%5Cnhttp://onlinelibrary.wiley.com/store/10.1029/92GL00938/asset/grl6087.pdf?v=1&t=hchlowx4&s=80c9c770e75a4184ef5e3dc0543c17040538da84.

Saunders WC, Bouwes N, McHugh P, Jordan CE. 2018. A network model for primary production highlights linkages between salmonid populations and autochthonous resources. Ecosphere 9:e02131. https://doi.org/10.1002/ecs2.2131.

Scown MW, McManus MG, Carson JH, Nietch CT. 2017. Improving predictive models of in-stream phosphorus concentration based on nationally-available spatial data coverages. JAWRA J Am Water Resour Assoc 53:944–60. https://doi.org/10.1111/1752-1688.12543.

Sinsabaugh RL, Repert D, Weiland T, Golladay SW, Linkins AE. 1991. Exoenzyme accumulation in epilithic biofilms. Hydrobiologia 222:29–37.

Smith RM, Kaushal SS. 2015. Carbon cycle of an urban watershed: exports, sources, and metabolism. Biogeochemistry 126:173–95.

Steinman AD, Lamberti G a., Leavitt PR. 2007. Biomass and pigments of benthic algae. In: Methods in stream ecology. pp 357–79.

Thorp JH, Thoms MC, Delong MD. 2006. The riverine ecosystem synthesis: biocomplexity in river networks across space and time. River Res Appl 22:123–47.

Thyssen N, Erlandsen M, Jeppesen E, Holm TF. 1983. Modelling the reaeration capacity of low-land streams dominated by submerged macrophytes. Dev Environ Modell 5:861–7.

Uehlinger U. 2006. Annual cycle and inter-annual variability of gross primary production and ecosystem respiration in a floodprone river during a 15-year period. Freshw Biol 51:938–50. https://doi.org/10.1111/j.1365-2427.2006.01551.x.

US-Geological-Survey. 2011. Office of Water Quality Technical Memorandum 2011.03 - Subject: Change to Solubility Equations for Oxygen in Water.

Val J, Chinarro D, Pino MR, Navarro E. 2016a. Global change impacts on river ecosystems: a high-resolution watershed study of Ebro river metabolism. Sci Total Environ 569:774–83.

Val J, Pino R, Navarro E, Chinarro D. 2016b. Addressing the local aspects of global change impacts on stream metabolism using frequency analysis tools. Sci Total Environ 569–570:798–814. http://linkinghub.elsevier.com/retrieve/pii/S0048969716313523.

Vannote RL, Minshall GW, Cummins KW, Sedell JR, Cushing CE. 1980. The river continuum concept. Can J Fish Aquat Sci.

Ver Hoef JM, Peterson E, Theobald D. 2006. Spatial statistical models that use flow and stream distance. Environ Ecol Stat 13:449–64. https://doi.org/10.1007/s10651-006-0022-8.

Ver Hoef JM, Peterson EE. 2010. A moving average approach for spatial statistical models of stream networks. J Am Stat Assoc 105:6–18.

Ver Hoef JM, Peterson EE, Clifford D, Shah R. 2014. SSN : an R package for spatial statistical modeling on stream networks. J Stat Softw 56:1–45. https://www.jstatsoft.org/index.php/jss/article/view/v056i03/v56i03.pdf.

Xu J, Yin W, Ai L, Xin X, Shi Z. 2016. Spatiotemporal patterns of non-point source nitrogen loss in an agricultural catchment. Water Sci Eng 9:125–33.

Young RG, Huryn AD. 1996. Interannual variation in discharge controls ecosystem metabolism along a grassland river continuum. Can J Fish Aquat Sci 53:2199–211. http://apps.webofknowledge.com.ep.fjernadgang.kb.dk/full_record.do?product=WOS&search_mode=GeneralSearch&qid=32&SID=R2Bt6jWCQ26BmocuH9Q&page=1&doc=1.

Young RG, Matthaei CD, Townsend CR. 2008. Organic matter breakdown and ecosystem metabolism: functional indicators for assessing river ecosystem health. J North Am Benthol Soc 27:605–25. https://doi.org/10.1899/07-121.1.